Geochemistry, Geophysics, Geosystems

RESEARCH ARTICLE
10.1029/2020GC009402

Key Points:

- The oceanic Suess effect disproportionately affects Subantarctic Mode Water (SAMW), within which $\delta^{13}C$ has decreased by c. −0.44‰ from 2008 to 2018
- The observed $\delta^{13}C$ change of −0.044‰/year represents roughly a 3-fold increase in the rate of $\delta^{13}C$ change compared to 1994–2008
- Between 2008 and 2018 SAMW in the SE Indian Ocean absorbed 5.5 ± 0.6 μmol/kg^{-1} of anthropogenic carbon per year

Supporting Information:

Supporting Information may be found in the online version of this article.

Correspondence to:

T. J. Williams,
thomas.williams@ufl.edu

Citation:

Williams, T. J., Wagner, A. J., Sikes, E. L., & Martin, E. E. (2021). Evolution of the oceanic ^{13}C Suess effect in the southeastern Indian Ocean between 1994 and 2018. *Geochemistry, Geophysics, Geosystems*, *22*, e2020GC009402. https://doi.org/10.1029/2020GC009402

Received 27 AUG 2020
Accepted 17 FEB 2021

Evolution of the Oceanic ^{13}C Suess Effect in the Southeastern Indian Ocean Between 1994 and 2018

Thomas J. Williams[1], Amy J. Wagner[2], Elisabeth L. Sikes[3], and Ellen E. Martin[1]

[1]Department of Geological Sciences, University of Florida, Gainesville, FL, USA, [2]Geology Department, California State University, Sacramento, CA, USA, [3]Department of Marine and Coastal Sciences, Rutgers University, New Brunswick, NJ, USA

Abstract The decrease in $\delta^{13}C$ of dissolved inorganic carbon ($\delta^{13}C_{DIC}$) owing to uptake of anthropogenic CO_2 (the oceanic ^{13}C Suess effect) in the Southeastern Indian Ocean over the last decade was calculated using an extended multiparameter linear regression technique. Samples collected on the CROCCA-2S (Coring to Reconstruct Ocean Circulation and Carbon Dioxide Across 2 Seas) cruise in November–December 2018 were compared to samples from the CLIVAR (Climate and Ocean: Variability, Predictability, and Change) and OISO (Océan Indien Service d'Observation) programs from 2007 to 2009. Surface ocean $\delta^{13}C_{DIC}$ decreased by an average of −0.53 ± 0.04‰ across this period, at an average rate of −0.053 ± 0.004‰ per year. This rate of $\delta^{13}C_{DIC}$ change is an increase from −0.021 ± 0.024‰ per year between 1994 and 2008. We find that the interior water mass most impacted by the oceanic ^{13}C Suess effect between 2008 and 2018 was Subantarctic Mode Water (SAMW), within which $\delta^{13}C_{DIC}$ decreased by −0.044 ± 0.002‰ per year. Using previously published relationships between the oceanic ^{13}C Suess effect and anthropogenic carbon, we estimate the annual storage of anthropogenic carbon within SAMW in the southeastern Indian Ocean has increased from ~2.0 ± 0.2 μmol/kg per year between 1994 and 2008 to 5.5 ± 0.6 μmol/kg per year between 2008 and 2018.

Plain Language Summary We measured the ratio of carbon isotopes within seawater to identify the amount of atmospheric carbon sourced from the burning of biomass and fossil fuels which has been absorbed into the southeastern Indian Ocean over the last decade. We find that the rate at which this human-sourced carbon is being absorbed by the ocean has increased up to 3-fold over this time period, when compared with the period between 1994 and 2008.

1. Introduction

The global utilization of fossil fuels for energy is rapidly increasing the CO_2 levels in the atmosphere, with the increase accelerating markedly in recent years (Dlugokencky et al., 2019; Raupach et al., 2007). The world's oceans are critical to the global carbon cycle, and contain 50 times more carbon than the atmosphere. The surface ocean rapidly exchanges carbon with the atmosphere and takes up a substantial portion of anthropogenic carbon in the process (Sabine et al., 2004). Formation of interior water masses and the resulting subsurface thermohaline circulation laterally transports waters ventilated at the surface through the ocean. The Southern Ocean is an important area for ocean-atmosphere gas exchange as part of the overturning thermohaline circulation. Here, deep water exported from the North Atlantic contributes to Circumpolar Deep Water (CDW) and is modified and ventilated during the formation of Antarctic intermediate and bottom water masses (Talley, 2013). CDW upwells in response to density and wind-driven divergence around Antarctica. At the surface a portion of these waters move northward, equilibrating CO_2 with the atmosphere, and converted too lower densities via addition of precipitation before being subducted (Hanawa & Talley, 2001; McCartney, 1977; Sloyan & Rintoul, 2001; Talley, 2013), sinking to form Antarctic Intermediate Water (AAIW) and Subantarctic Mode Water (SAMW). The Indian Ocean sector of the Southern Ocean is an important site globally for the formation of these intermediate-depth water masses (McCartney, 1977; Talley, 2013).

The carbon isotope composition of atmospheric CO_2 and that of the dissolved inorganic carbon (DIC) in the surface ocean can provide valuable constraints on the carbon cycle (e.g., Keeling et al., 2005). The stable isotope composition of DIC in the surface ocean reflects the balance between fractionation during dissolution

from the atmosphere and the preferential uptake of the lighter isotope of carbon, ^{12}C, during fixation in the photosynthetic process (Freeman & Hayes, 1992; O'Leary, 1981). The carbon in anthropogenic CO_2 has an original photosynthetic source, consequently its isotopic signal also reflects fractionation during fixation in the photosynthetic process. Owing to this photosynthetic source, the carbon isotope composition, or $\delta^{13}C$, of CO_2 released during the combustion of fossil fuels and biomass burning is very negative, about −30‰. Prior to the industrial revolution, $\delta^{13}C$ of atmospheric CO_2 was −6.7‰ (H. Graven et al., 2017). Addition of this isotopically negative anthropogenic carbon into the atmosphere means that $\delta^{13}C$ of CO_2 in the atmosphere today is around −8.5‰. This anthropogenic perturbation in the $\delta^{13}C$ of atmospheric CO_2 is referred to as the ^{13}C Suess effect, or the oceanic ^{13}C Suess effect when referring to its expression in the ocean (Keeling et al., 1979).

The oceanic ^{13}C Suess effect is of interest because it provides useful constraints on the size of the oceanic sink of anthropogenic carbon, as well as a means for estimating the rate of the ocean's uptake of anthropogenic CO_2 (e.g., Eide, Olsen, Ninnemann, & Eldevik, 2017; Quay et al., 1992; Sonnerup et al., 1999). The usefulness of the $\delta^{13}C$ of DIC ($\delta^{13}C_{DIC}$) as a tracer results from the difference between the $\delta^{13}C$ of CO_2 in the atmosphere ($\delta^{13}C_{atm}$, presently around −8.5‰) and that of the surface ocean (i.e., $\delta^{13}C_{DIC}$), around 0–2‰ (Quay et al., 2017). The air-sea $^{13}CO_2$ flux caused by addition of anthropogenic carbon can be more accurately determined than total carbon flux because, unlike the air-sea CO_2 flux, the $\delta^{13}C$ gradient across the air-sea interface is large relative to its variability and can be more accurately determined with limited measurements (Quay et al., 2007). The ability to detect an anthropogenic $\delta^{13}C$ change in the ocean is also greater than for the change in DIC itself (Quay et al., 1992, 2003; Tans et al., 1993).

One effective way to estimate changes in the oceanic ^{13}C Suess effect is by comparing two individual data sets collected in the same region but at different times (e.g., Gruber et al., 1999; Quay et al., 1992; Sonnerup et al., 1999, 2000). Although this method necessarily has some aliasing due to seasonal, spatial, and interannual variability, this approach has illuminated substantial regional variations in the oceanic ^{13}C Suess effect (e.g., Eide, Olsen, Ninnemann, & Johannessen, 2017; Quay et al., 2007, 2017). Subsurface changes have been shown to reflect circulation and ventilation of the ocean (e.g., Eide, Olsen, Ninnemann, & Johannessen, 2017). For example, the surface and subsurface in the southeastern Indian Ocean—along with the North Atlantic, southeastern Pacific and northern Pacific—appear to have been disproportionately affected by the oceanic ^{13}C Suess effect (Eide, Olsen, Ninnemann, & Johannessen, 2017). In addition to identifying regions of anthropogenic CO_2 uptake by the oceans, this method has been used to investigate temporal variability in uptake. Previous studies have suggested that anthropogenic CO_2 uptake in the Southern Ocean has been accelerating since the early 2000s (Landschützer et al., 2015; Quay et al., 2017).

In this study, we present new $\delta^{13}C_{DIC}$ data collected from the southeast Indian Ocean and Southern Ocean as part of the Coring to Reconstruct Ocean Circulation and Carbon Dioxide Across 2 Seas (CROCCA-2S) cruise in November–December 2018. To separate natural from anthropogenic changes in $\delta^{13}C_{DIC}$, we model predicted $\delta^{13}C_{DIC}$ values based on data collected from the same region in 2007–2009. The deviation in our data from these modeled $\delta^{13}C_{DIC}$ values is attributed to the oceanic ^{13}C Suess effect (McNeil et al., 2001; Quay et al., 2007; Sonnerup et al., 2000). We find that over the last decade annual rates of anthropogenic CO_2 absorption have increased nearly 3-fold compared with the period between 1994 and 2009.

2. Materials and Methods

2.1. Sample Collection and Carbon Isotope Analyses

The $\delta^{13}C_{DIC}$ depth profiles at 22 stations were collected on the CROCCA-2S cruise to the Southeast Indian Ocean in November–December 2018 (Figures 1 and 2). $\delta^{13}C_{DIC}$ represents the $\delta^{13}C$ of DIC where $\delta^{13}C$ (‰) = $[(^{13}C/^{12}C)_{sample}/(^{13}C/^{12}C)_{standard} - 1] * 1000$, reported against Vienna Pee Dee Belemnite (VPDB). The methods for collection and measurement of the $\delta^{13}C_{DIC}$ during our cruise follow those of previous work (e.g., Kroopnick, 1985; Quay et al., 1992). Seawater samples, poisoned with $HgCl_2$, were collected and stored in prewashed and baked (500°C) ground glass-stoppered bottles.

Carbon isotopic ratios of DIC were measured with a Thermo Finnigan DeltaPlus XL isotope ratio mass spectrometer with a GasBench II universal on-line gas preparation device at the University of Florida's Stable Isotope Lab. Water was injected into septum top vials that contained 0.5 ml phosphoric acid and

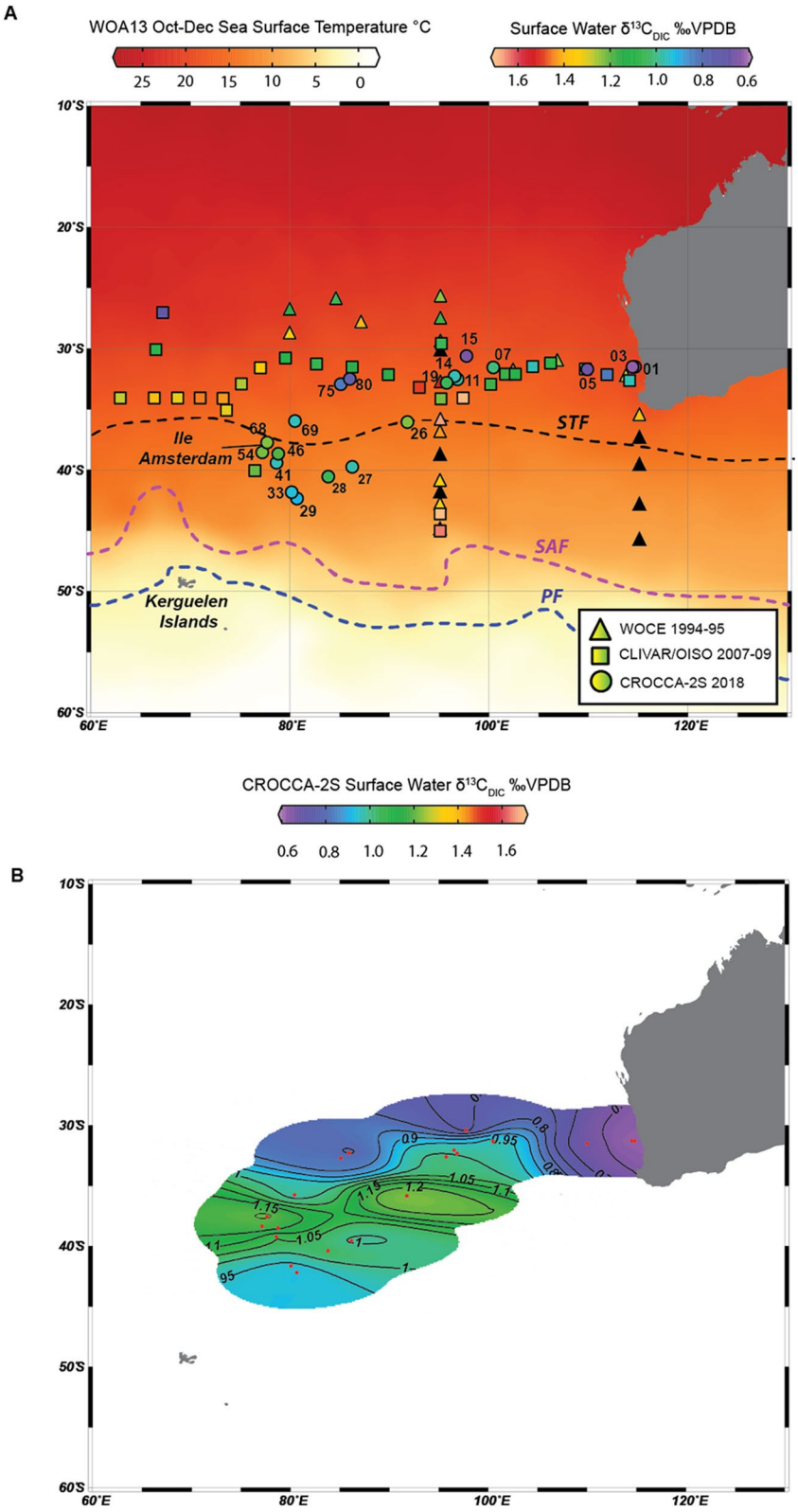
A
WOA13 Oct-Dec Sea Surface Temperature °C
25 20 15 10 5 0
Surface Water δ13CDIC ‰VPDB
1.6 1.4 1.2 1.0 0.8 0.6
10°S
20°S
30°S
40°S
50°S
60°S
60°E
80°E
100°E
120°E
STF
SAF
PF
Ile Amsterdam
Kerguelen Islands
WOCE 1994-95
CLIVAR/OISO 2007-09
CROCCA-2S 2018
CROCCA-2S Surface Water δ13CDIC ‰VPDB
0.6 0.8 1.0 1.2 1.4 1.6
B

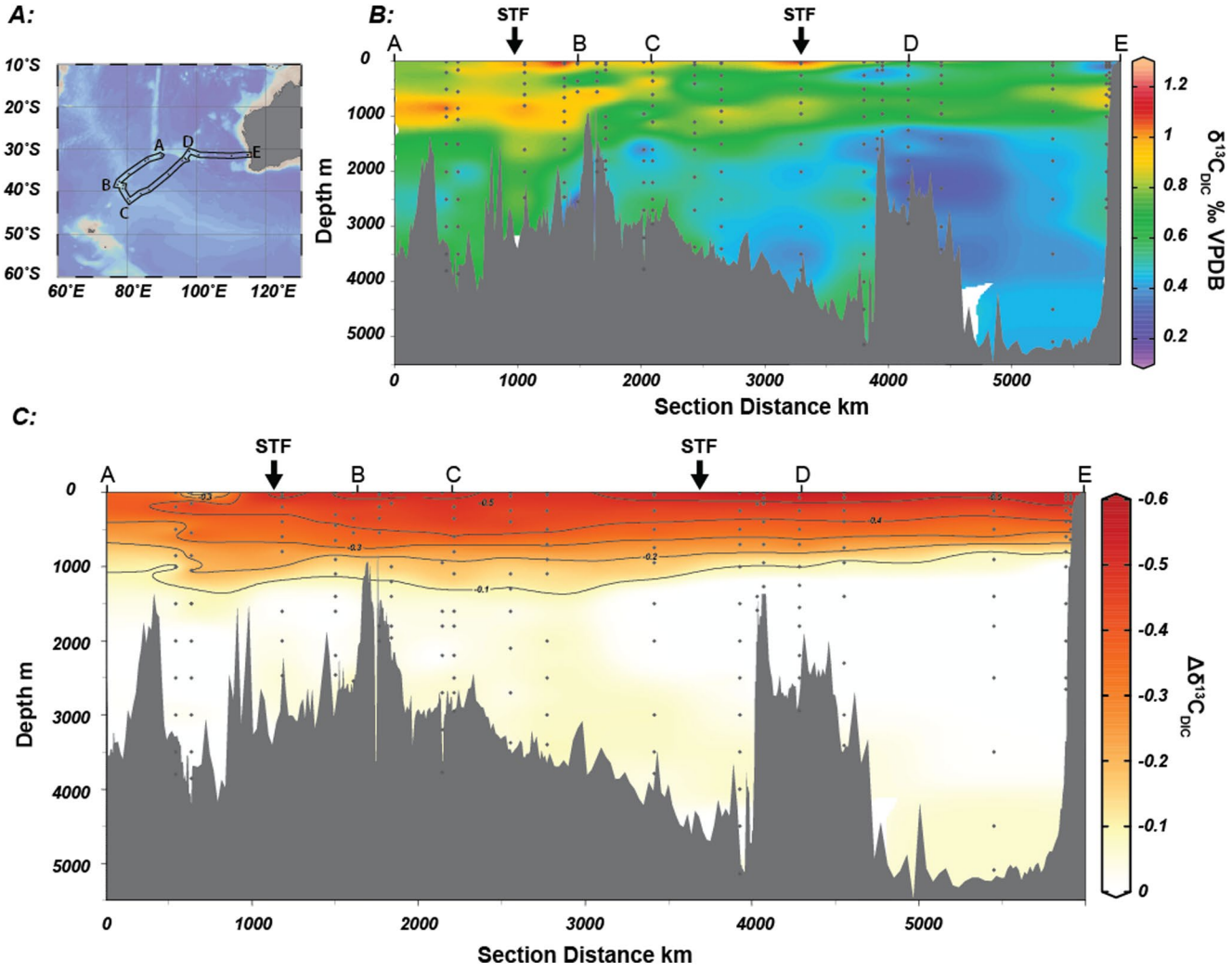

Figure 2. (a) Location of CROCCA-2S cruise in November–December 2018. (b) Cross-section of CROCCA-2S $\delta^{13}C_{DIC}$. Location of cross-section shown in (a). (c) Change in $\delta^{13}C_{DIC}$ since CLIVAR and OISO cruises in 2007–2009 due to the oceanic ^{13}C Suess effect ($\Delta\delta^{13}C_{DIC}$) estimated using an extended multiple linear regression method (see Section 2). Arrows in panels (b) and (c) illustrate the approximate location of Subtropical Front at the time data was collected. Figure produced using Ocean Data View (Schlitzer, 2019).

were filled with helium. This acidification released all DIC into the headspace and the mixture of CO_2 and He was sampled by the GasBench II where CO_2 and any N_2 were separated by a GC column prior to being measured on the mass spectrometer. An in-house $KHCO_3$ standard was utilized for these analyses, which is prepared weekly by dissolution of solid $KHCO_3$ in deionized water to a concentration of 24 mg of C pre ml, approximate to the concentration of C within seawater. The $KHCO_3$ standard has been isotopically characterized for $\delta^{13}C$ via two methods: first, via acidification of phosphoric acid with resultant CO_2 measured verses international standards NBS-19, NBS-18 using two different carbonate isotopes instruments—a Kiel carbonate prep devise 252 IRMS and common acid bath VG PRISM IRMS. Second, via combustion in an elemental analyzer with resultant CO_2 measured versus international standards USGS40 and USGS41 using a Costech ESC 4010 elemental analyzer—Thermo DeltaPlusXL IRMS, and also a Carlo Erba NA1500

Figure 1. (a) Map of modeled sea surface temperature from the southeast Indian and Southern oceans in October–December, from World Ocean Atlas 2013 (Locarnini et al., 2013). Overlain are locations of CROCCA-2S, CLIVAR 2007–2009 (Feely, Dickson, et al., 2013; Feely, Sabine, Dickson, et al., 2013; Feely, Sabine, Millero, et al., 2013), OISO 2009 (Metzl & Lo Monaco, 2018), and WOCE 1994/95 (Talley et al., 2013) stations colored by surface water $\delta^{13}C_{DIC}$. Numbers correspond to CROCCA-2S station numbers. Back triangles indicate WOCE stations with no surface (0–30 m) $\delta^{13}C_{DIC}$ data. The approximate location of the Subtropical, Subantarctic, and Polar fronts are also shown (STF, SAF, and PF, respectively). (b) Contoured CROCCA-2S surface water $\delta^{13}C_{DIC}$. Figure produced using Ocean Data View (Schlitzer, 2019).

elemental analyzer—Thermo Delta V Advantage IRMS. The overall precision of the $\delta^{13}C$ analysis was ±0.02‰ based on replicate analyses of standards and seawater samples.

2.2. Modeling Predicted $\delta^{13}C_{DIC}$

To quantify recent changes in the oceanic ^{13}C Suess effect, we compared data collected during CROCCA-2S with previously published measurements from the area. For this comparison, we compiled data from the Climate and Ocean: Variability, Predictability and Change program (CLIVAR) lines I05, I08S, I09N, and the Océan Indien Service d'Observation program (OISO) line OISO-17 (henceforth collectively referred to as the CLIVAR data set) that were occupied in 2007–2009 (Feely, Dickson, et al., 2013; Feely, Sabine, Dickson, et al., 2013; Feely, Sabine, Millero, et al., 2013; Metzl & Lo Monaco, 2018). To isolate the anthropogenic component of any $\delta^{13}C_{DIC}$ change since 2007–2009, we model predicted $\delta^{13}C_{DIC}$ values ($\delta^{13}C_{DIC\text{-}P}$) for the 2018 CROCCA-2S data set using the CLIVAR data set, assuming no Suess effect. For this calculation, we utilized the close correlation of $\delta^{13}C_{DIC}$ with potential temperature (θ), salinity (S), apparent oxygen utilization (AOU), and nitrate (N) (Wallace, 1995). We performed a multiple linear regression (MLR) of the CLIVAR data set using θ, S, AOU and N as independent variables and $\delta^{13}C_{DIC}$ as the dependent variable. The intercept (β) and coefficients (m) of this analysis were then applied to our θ, S, AOU, and N data to compute $\delta^{13}C_{DIC\text{-}P}$ after Quay et al. (2017):

$$\delta^{13}C_{DIC\text{-}P\text{-}CLIVAR} = \beta + m_1\theta + m_2S + m_3\mathrm{AOU} + m_4N$$

The same multivariate analyses was also performed on the CROCCA-2S data set:

$$\delta^{13}C_{DIC\text{-}P\text{-}CROCCA\text{-}2S} = \beta + M_1\theta + M_2S + M_3\mathrm{AOU} + M_4N$$

Both sets of predictive coefficients (m_1–m_4 and M_1–M_4) were then applied to the CROCCA-2S data set, with the difference between the two predicted $\delta^{13}C_{DIC}$ values attributed to the oceanic ^{13}C Seuss effect between the two time periods ($\Delta\delta^{13}C$):

$$\Delta\delta^{13}C = \left(\beta + M_1\theta + M_2S +_3 \mathrm{AOU} + M_4N\right) - \left(\beta + m_1\theta + m_2S + m_3\mathrm{AOU} + m_4N\right)$$

This technique, known as extended multiple linear regression (eMLR), has been shown to minimize scatter in $\Delta\delta^{13}C_{DIC}$ estimates introduced by outliers (Friis et al., 2005). The same eMLR was also performed on World Ocean Circulation Experiment (WOCE) data collected during 1994–1995 from this region (Talley et al., 2013) and the 2007–2009 CLIVAR data set to determine $\Delta\delta^{13}C_{DIC}$ between 1994–1994 and 2007–2009. Uncertainties in eMLR $\Delta\delta^{13}C_{DIC}$ are the standard error of each MLR and analytical error summed in quadrate. Errors are ±0.21‰ for the eMLR between 2008 and 2018 and ±0.024‰ between 1994 and 2008. Analytical error is an order of magnitude smaller than MLR standard errors, which stem from scatter within both the independent and dependent variables.

We follow the eMLR method of Friis et al. (2005) in retaining data from the upper 100 m of the water column in our calculations. Incorporating surface waters increases the standard error of the resulting MLR due to less linearity in independent variables, for example due to complete utilization of nutrients within the surface ocean at some stations. However, excluding the upper 100 m of the water column introduces systematic bias in $\Delta\delta^{13}C_{DIC}$ at waters below 2,000 m—where the ^{13}C Suess effect should be minimal or nonexistent—toward ^{13}C-depleted values, and so yields a less accurate $\Delta\delta^{13}C_{DIC}$ (Figure S1).

The predictive variables used in these analyses are not entirely independent of one another, thereby introducing a degree of multicollinearity. One may expect collinearity to especially be an issue for AOU and N, given the mechanistic link between the two. However, previous studies have demonstrated these variables to be most effective at modeling oceanic carbon and $\delta^{13}C_{DIC}$ distributions (e.g., Sonnerup et al., 2000). Moreover, the exclusion of AOU or N from our MLR increases standard error, suggesting collinearity is not an issue in this instance. We limited the included CLIVAR and WOCE data to stations in the immediate vicinity of our cruise (25°S to 45°S; 60°E-120°E) in order to constrain water mass variability. The inclusion of cruise

tracks from multiple years (i.e., 2007–2009) within a single eMLR increases error, however is necessary in order to incorporate data from a wide enough geographical area to properly characterize spatial variability in physical properties, nutrients, and $\delta^{13}C_{DIC}$. Moreover, incorporating multiple years of data also means the data set is more likely to reflect natural temporal variability which may otherwise have been missed. In total, we incorporated 811 CLIVAR casts across 29 stations and 406 WOCE casts across 19 stations (Figure 1).

3. Results

3.1. Surface $\delta^{13}C_{DIC}$ Distributions in the SE Indian Ocean

The CROCCA-2S cruise track took us from subtropical waters in late austral spring (November), across the STF and into subantarctic waters, and back to subtropical waters in early austral summer (December). Most sites sat north of the STF, with sites 27, 28, 29, and 33 located south of the front (as determined by SST gradients) and sites 26, 41, 46, 54, 68, and 69 situated within the frontal zone (Figure 1a). $\delta^{13}C_{DIC}$ of surface waters in the north of the study area show a general trend of increasing southwards toward the STF, from ~0.6‰ at c. 31°S to ~1.2‰ at the front itself (Figure 1b). This is followed by a decrease to 0.92‰ within subantarctic waters at c. 42°S. The elevated $\delta^{13}C$ values at the STF are most likely due to biological productivity concentrated at the front during the spring bloom. This observation is in agreement with CTD fluorescence data (a proxy for water chlorophyll content) which recorded up to a fivefold increase in surface water fluorescence values between −30°S and c. 36°S–40°S, followed by a decrease at −42°S (Figure S1). We also saw visual evidence of this bloom in the coloration of the surface water during sampling.

The CROCCA-2S surface $\delta^{13}C_{DIC}$ data were consistently lower than both WOCE and CLIVAR data (Figure 1a). Although CLIVAR data are somewhat restricted in latitudinal coverage, there is a general trend toward higher surface water values to the south, with maxima around −44°S, which is similar to the latitudinal pattern observed in the CROCCA-2S data set.

3.2. Sub-Surface $\delta^{13}C_{DIC}$ Distributions in the SE Indian Ocean

Subsurface CROCCA-2S $\delta^{13}C_{DIC}$ data are characterized by ^{13}C-enrichment maxima between c. 400–1,500 m water depth (Figure 2b), peaking at c. 600–900 m. Waters within this maxima have $\delta^{13}C_{DIC}$ values up to 0.43‰ greater than the overlying surface water, except in the vicinity of the STF, where the highest values are found in surface waters (Figures 1 and S2). The highest subsurface $\delta^{13}C_{DIC}$ values of up to 1.13‰ were found between 600 and 1,200 m water depth between 37.5°S and 31.5°S, in the immediate vicinity and just north of the STF (line A–B in Figure 2b). This is slightly deeper than the maximum found to the north and east (line D–E and parts of C–D in Figure 2b). The depth of this maximum correlated well with the depth of the core of the AAIW in this region of the ocean (defined by the salinity minimum, see Figure S3) which progressively shallows to the north in this region across these latitudes (Talley et al., 2013).

Below this AAIW-depth maxima, $\delta^{13}C_{DIC}$ values decrease and are regionally variable. Within the Perth Basin immediately west of Australia, a $\delta^{13}C_{DIC}$ low of 0.3–0.22‰ is centered around 2,200–2,300 m water depth (line D–E in Figure 2b). This corresponds with the core of Upper Circumpolar Deep Water (UCDW), characterized by isoneutral contours Υ^N = 27.8–28.04 kg/m^3 and an oxygen minimum (O_2 = <180 umol/kg^{-1}; Talley, 2013). This O_2 minimum is imparted by return flow of Indian Deep Water (IDW), which flows southward at depths of 2,000–2,500 m along the eastern flank of the Indian Ocean (Tamsitt et al., 2019). IDW is rich in remineralized carbon and correspondingly less enriched in ^{13}C (Talley et al., 2013), leading to the $\delta^{13}C_{DIC}$ minimum we observed in the east of our study region, particularly within the Perth Basin.

Immediately south of Broken Ridge (line C–D in Figure 2b), there is a relatively ^{13}C-enriched abyssal water mass between c. 3,500–5,000 m water depth ($\delta^{13}C_{DIC}$ = 0.60‰). This water mass is Lower Circumpolar Deep Water (LCDW), characterized in this region by an *S*-maxima at depth (Talley, 2013). A degree of mixing between LCDW and AABW south of Broken Ridge is suggested by the relatively high oxygen content of these waters (O_2 = >200 umol/kg^{-1}) and lower S (*S* = 34.71) than overlying pure LCDW (S_{max} = 34.74, Talley, 2013). LCDW ($\delta^{13}C_{DIC}$ = 0.64‰) is also observed at c. 4,000 m water depth further west, where it flows eastward within the deep channel between Broken Ridge and the Southeast Indian Ridge (c. 500 km along

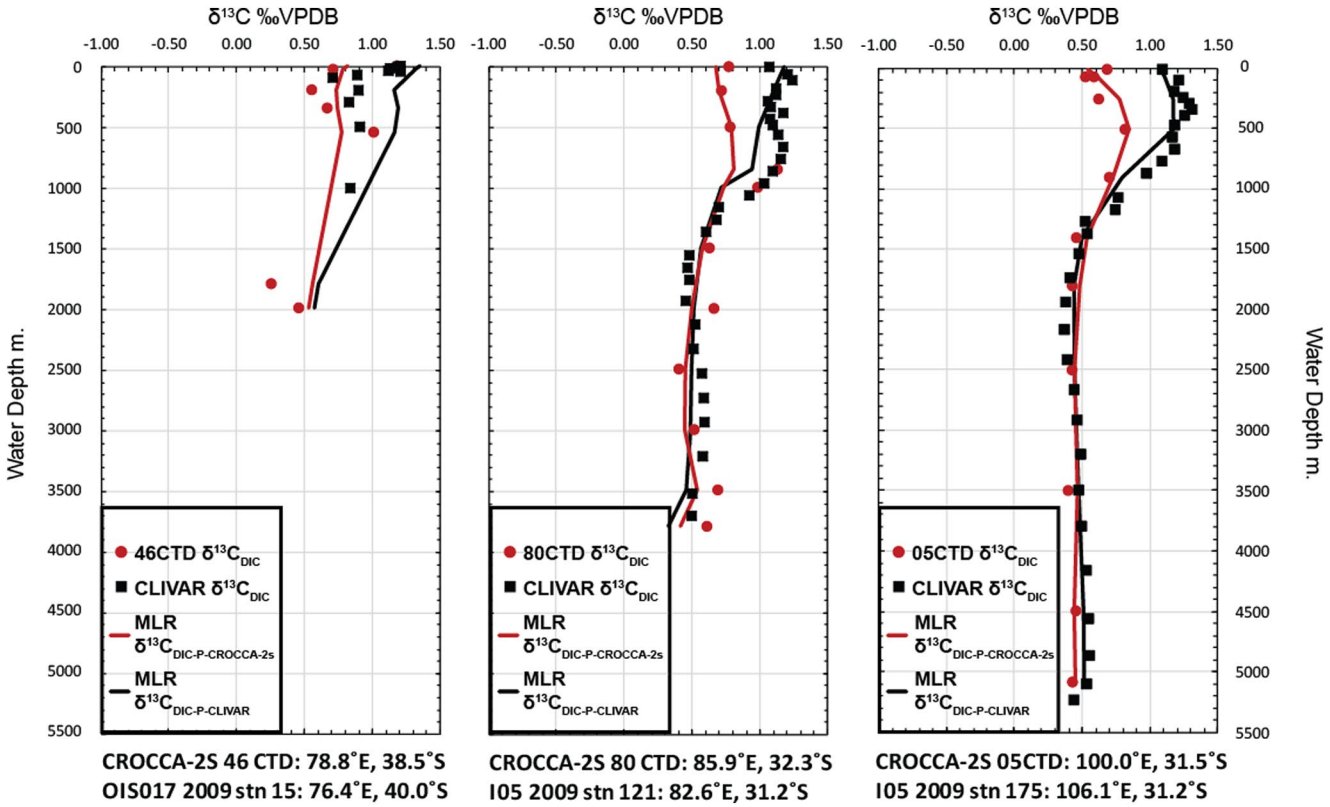

Figure 3. Representative $\delta^{13}C_{DIC}$ profiles from three CROCCA-2S stations (red dots) alongside nearby CLIVAR and OISO stations (black squares; Feely, Dickson, et al., 2013; Metzl & Lo Monaco, 2018). The red line represents the MLR-predicted $\delta^{13}C_{DIC}$ for each CROCCA-2S station, modeled using the entire CROCCA-2S data set. The black line is the MLR-predicted $\delta^{13}C_{DIC}$ for CROCCA-2S stations modeled using CLIVAR and OISO data. The difference between the MLR-predicted values represents the eMLR modeled $\delta^{13}C_{DIC}$ change due to the oceanic ^{13}C Suess effect (see Section 2).

section in Figure 2b). LCDW within this passage is lower in oxygen content ($O_2 = 189$ umol/kg) and slightly more saline ($S = 34.73$) than LCDW found south of Broken Ridge, likely due to less mixing with AABW.

4. Discussion

4.1. Change in $\delta^{13}C_{DIC}$ Between 2007–2009 and 2018

The change in $\delta^{13}C_{DIC}$ with time can be illustrated by comparing CROCCA-2S $\delta^{13}C_{DIC}$-depth profiles with nearby measurements made along CLIVAR line I05 and OISO line 17 during 2009, where they exist. It is readily apparent that $\delta^{13}C_{DIC}$ measurements in the upper 500–800 m of the water column made during the 2018 CROCCA-2S cruise are up to 0.95‰ lower than those from 2009 (Figure 3). The difference in $\delta^{13}C_{DIC}$ between 2009 and 2018 appears restricted to the upper 1,000 m of the water column. However, locations where coincident CLIVAR and CROCCA-2S $\delta^{13}C_{DIC}$ data exist are limited (Figure 1).

Although there is a clear pattern of lower $\delta^{13}C_{DIC}$ within the upper water column of the CROCCA-2S data set compared to the CLIVAR data, it is difficult to quantify the extent that this difference can be attributed to the ^{13}C Suess effect using a direct comparison of nearby stations. A direct comparison between CLIVAR and CROCCA-2S data is further hampered by the relatively few stations within close proximity to one another. $\delta^{13}C_{DIC}$ can vary as a function of air and sea surface temperature (SST) during air-sea gas exchange, with colder temperatures enhancing fractionation (Zhang et al., 1995). The preferential uptake of ^{12}C over ^{13}C during biological productivity increases the $\delta^{13}C_{DIC}$, and remineralization of this biological carbon at depth reverses the process. These effects can mask an assessment of transient changes in $\delta^{13}C_{DIC}$ related to the oceanic ^{13}C Suess effect. In order to determine the extent of changes between 2007–2009 and 2018 attributable to the oceanic ^{13}C Suess effect, we performed an eMLR of CLIVAR and CROCCA-2S data to model

Table 1
Depth-Binned $\Delta\delta^{13}C_{DIC}$ Between 2007–2009 and 2018, and Annual Change in $\Delta\delta^{13}C_{DIC}$ Between 1994–2008 and 2008–2018

Depth (m)	2008–2018 $\Delta\delta^{13}C_{DIC}$	*n*	S.D.	2008–2018 $\Delta\delta^{13}C_{DIC}$/yr	1994–2008 $\Delta\delta^{13}C_{DIC}$/yr	1994–2008 $\Delta\delta^{13}C_{DIC}$/yr offset applied
0–49	−0.53 ± 0.04	23	0.02	−0.053 ± 0.004	−0.013 ± 0.002	−0.025 ± 0.002
50–149	−0.53 ± 0.06	11	0.02	−0.053 ± 0.006	−0.010 ± 0.002	−0.023 ± 0.002
150–299	−0.44 ± 0.05	17	0.03	−0.044 ± 0.005	−0.007 ± 0.002	−0.020 ± 0.002
300–499	−0.42 ± 0.06	12	0.04	−0.042 ± 0.006	−0.004 ± 0.002	−0.017 ± 0.002
500–749	−0.32 ± 0.05	19	0.07	−0.032 ± 0.005	−0.001 ± 0.002	−0.014 ± 0.002
750–999	−0.17 ± 0.06	14	0.08	−0.017 ± 0.006	0.005 ± 0.002	−0.008 ± 0.002
1,000–1,499	−0.05 ± 0.05	19	0.09	−0.005 ± 0.006	0.010 ± 0.002	−0.003 ± 0.002
1,500–1,999	0.00 ± 0.05	20	0.04	0.000 ± 0.005	0.011 ± 0.002	−0.002 ± 0.002
2,000–2,999	−0.01 ± 0.04	31	0.07	−0.001 ± 0.004	0.012 ± 0.002	−0.001 ± 0.002
3,000–3,999	−0.03 ± 0.05	19	0.06	−0.003 ± 0.005	0.013 ± 0.002	0.001 ± 0.002
>4,000	−0.05 ± 0.09	5	0.04	−0.005 ± 0.009	0.014 ± 0.002	0.001 ± 0.002

Note. An offset of 0.14‰ has been applied to 1994 data used in calculating annual change; also shown are data with no offset. Errors are propagated uncertainty in $\delta^{13}C_{DIC}$ calculations. Data also shown in Figure 5.

predicted $\delta^{13}C_{DIC}$ for our cruise, based on physical and biological parameters ($\delta^{13}C_{DIC\text{-}P}$, see Section 2). The residuals within this model ($\Delta\delta^{13}C_{DIC}$; i.e., the difference between red and black curves in Figure 3) quantify the oceanic ^{13}C Suess effect for the decade between ~2008 and 2018 (Figure 2c).

$\Delta\delta^{13}C_{DIC}$ is greatest in the eastern and southern section of the CROCCA-2S cruise transect (c. 1,500–5,800 km along section in Figure 2c), where residual values of up to −0.57 ± 0.21‰ are recorded within the upper 100 m of the water column. $\Delta\delta^{13}C_{DIC}$ is greatest in the surface mixed layer and decreases linearly with depth to ~1,250–1,500 m water depth (Figure 2c). An inflection point in the trend of $\Delta\delta^{13}C_{DIC}$ versus depth occurs at ~1,250–1,500 m water depth, with data below 1,500 m clustering around an average value of −0.02 ± 0.03‰. This depth corresponds approximately to the base of AAIW within this region, and the changing trend of $\Delta\delta^{13}C_{DIC}$ suggests the base of this water mass is the lower limit of waters affected by the oceanic ^{13}C Suess effect within the study area. AAIW and SAMW (which overlays AAIW) originate within the Polar and Subpolar surface ocean (Sallée et al., 2010). CDW below SAMW and AAIW are expected to have remained out of contact with the atmosphere since the prior to the industrial revolution (Fine, 1993). The observation that average $\Delta\delta^{13}C_{DIC}$ values below the lower limits of AAIW (below ~1,000–1,500 m) are within error of 0‰ therefore lends confidence to the assertion that $\Delta\delta^{13}C_{DIC}$ represents changes due to the oceanic ^{13}C Suess effect (Table 1).

Within the southeastern Indian Ocean isopycnals are tilted due to the formation, sinking and northward advection of SAMW and AAIW as well as upwelling of CDW within the Southern Ocean. Additional vertical and horizontal variability in the region of this study is caused by routing of water masses around and over bathymetry, for example in the region of Ile Amsterdam (near B in cross-section Figure 2c) and Broken Ridge (c. 250 m along section in Figure 2c) (McCartney & Donohue, 2007). In an area with complex bathymetry and ocean dynamics, depth is therefore not a reliable determinant of water mass. Temperature and salinity are conservative tracers used for identifying water masses within the ocean interior, making it useful to examine $\delta^{13}C_{DIC}$ and $\Delta\delta^{13}C_{DIC}$ in potential temperature-salinity (T-S) and density space (Figure 4). CROCCA-2S data fall within the same T-S space as CLIVAR data (black dots in Figures 4a–4d), indicating that the range of water mass physical properties incorporated into the eMLR used in this study is representative of the water masses sampled during the CROCCA-2S cruise.

The highest CROCCA-2S $\delta^{13}C_{DIC}$ values of 1.19–1.23‰ occur within surface waters with relatively low salinity and temperatures (θ = 16.2–17.6°, S = 35.22–35.36; Figure 4a). Within our cruise area this is indicative of waters found in the region just south of the STF (stations 26, 46, and 68, Figure 1). In contrast, $\Delta\delta^{13}C_{DIC}$

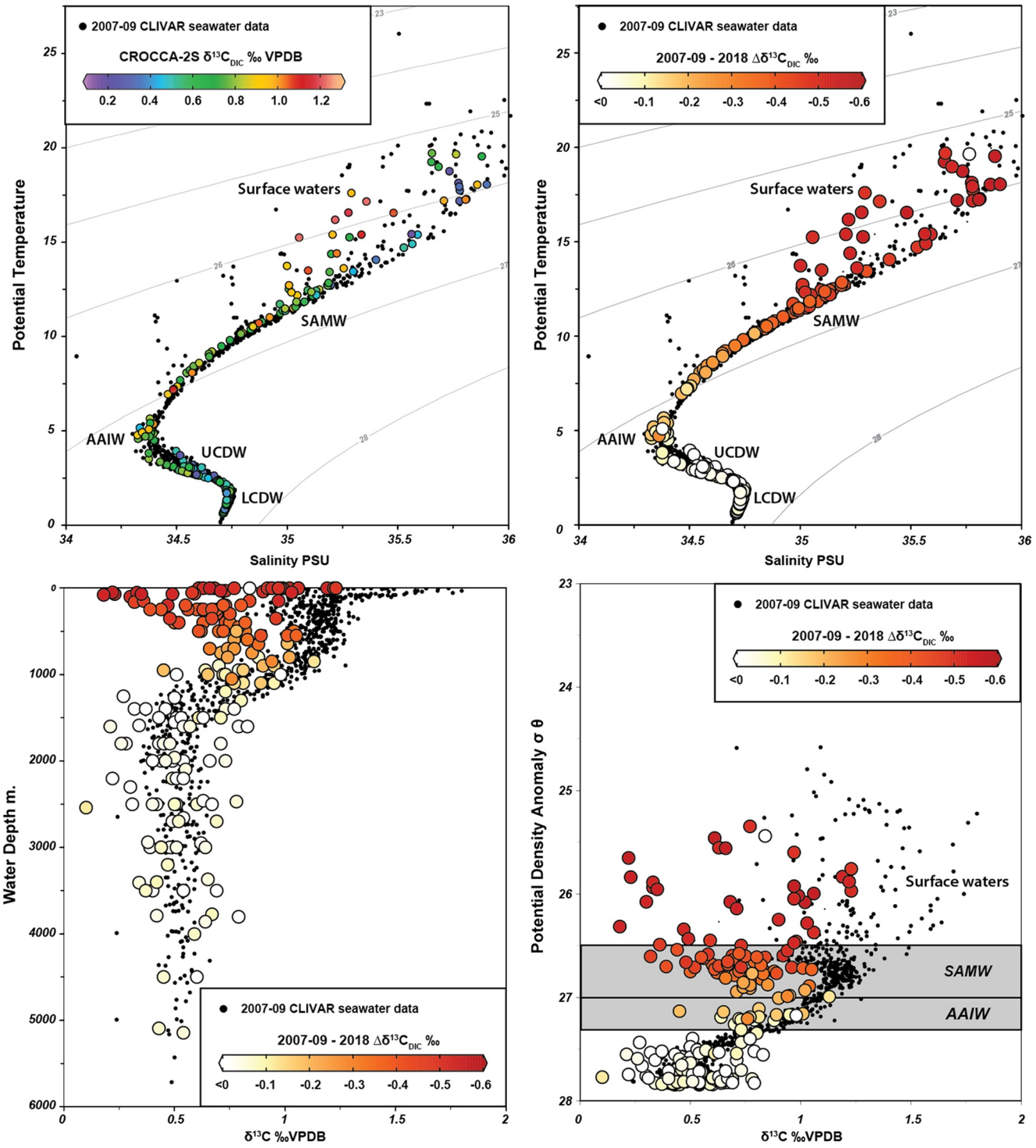

Figure 4. (a) T-S plot of CLIVAR/OSIO 2007–2009 data (Feely, Dickson, et al., 2013; Feely, Sabine, Dickson, et al., 2013; Feely, Sabine, Millero, et al., 2013; Metzl & Lo Monaco, 2018) used in eMLR analyses overlain by CROCCA-2S data colored by $\delta^{13}C_{DIC}$. (b) T-S plot of CLIVAR/OSIO 2007–2009 data used in eMLR analyses overlain by CROCCA-2S data. CROCCA-2S data colored by deviation of $\delta^{13}C_{DIC}$ measurements from predicted values, attributed to the oceanic ^{13}C Suess effect ($\Delta\delta^{13}C_{DIC}$). T-S distributions suggest sampling of the same water masses within both data sets. (c) Depth profile of CLIVAR/OSIO and CROCCA-2S $\delta^{13}C_{DIC}$ values demonstrating the differences in $\delta^{13}C_{DIC}$ in surface and subsurface water masses between the two data sets. (d) $\delta^{13}C_{DIC}$ versus potential density anomaly plot with Subantarctic Mode Water (SAMW) and Antarctic Intermediate Water (AAIW) shaded (Talley et al., 2011). The largest $\Delta\delta^{13}C_{DIC}$ is found in surface waters and SAMW, suggesting the ^{13}C Suess effect has had the greatest impact on these waters. Figure produced using Ocean Data View (Schlitzer, 2019).

Table 2
Estimates of the Oceanic ^{13}C Suess Effect ($\Delta\delta^{13}C_{DIC}$) and Anthropogenic Carbon Storage ($\Delta[C_{anth}]$) for Specific Isopycnal Ranges

Potential density layer	2008–2018 $\Delta\delta^{13}C_{DIC}$	N	S.D.	Eide, Olsen, Ninnemann, and Eldevik (2017) calculated slope ‰ (μmol kg^{-1})	2008–2018 $\Delta[C_{ant}]$ μmol/kg^{-1}	Water mass
<26.5	−0.53 ± 0.04	34	0.03	–	–	Surface
26.5–26.7	−0.44 ± 0.05	21	0.04	−0.008	55 ± 6	SAMW
26.7–26.9	−0.33 ± 0.04	27	0.07	−0.014	24 ± 3	SAMW
26.9–27.1	−0.20 ± 0.08	7	0.05	−0.024	8 ± 3	SAMW/AAIW interface
27.1–27.3	−0.11 ± 0.05	16	0.06	−0.022	5 ± 2	AAIW
27.3–27.5	−0.01 ± 0.08	7	0.05	−0.016	1 ± 5	CDW
27.5–27.7	0.00 ± 0.04	26	0.05	−0.018	0 ± 2	CDW
>27.7	−0.02 ± 0.03	52	0.06	–	–	CDW

Note. $\Delta[C_{anth}]$ was calculated based on the relationship between $\Delta\delta^{13}C_{DIC}$ and $\Delta[C_{anth}]$ for specific isopycnals calculated by Eide, Olsen, Ninnemann, and Eldevik (2017). Errors reflect uncertainty in binned $\Delta\delta^{13}C_{DIC}$. $\Delta[C_{ant}]$ errors do not take into account uncertainty in slopes calculated by Eide, Olsen, Ninnemann, and Eldevik (2017) and are thus likely to under estimate total uncertainty. NB, no relationship was calculated by Eide, Olsen, Ninnemann, and Eldevik (2017) for potential density layers $\sigma\theta$ = <26.5 and $\sigma\theta$ = >27.7.

values are greatest (up to −0.57 ± 0.21‰) within the surface mixed layer (c. 0–100 m depth) with higher temperatures and salinities (θ > 15.4–18.6, S > 35.48), within SAMW pycnocline waters (Figure 4b).

In density space CROCCA-2S deep water (i.e., sub-AAIW; potential density σ_θ = >27.35, Talley et al., 2011) $\delta^{13}C_{DIC}$ largely falls along the same array as CLIVAR data (Figure 4d). Moreover, $\Delta\delta^{13}C_{DIC}$ clusters around zero (average = −0.01 ± 0.02‰) at densities of σ_θ = >27.35. This is due to these denser water masses (i.e., UCDW/LCDW) remaining isolated from the atmosphere and thus isolated from changes owing to the ^{13}C Suess effect. CROCCA-2S $\delta^{13}C_{DIC}$ shifts toward lower values than CLIVAR data within AAIW (σ_θ = 27.0–27.35, Talley et al., 2011), nearly all SAMW (σ_θ = 26.0–27.0, Talley et al., 2011) and surface/subsurface waters (σ_θ = <26.0). The largest $\Delta\delta^{13}C_{DIC}$ is observed in surface and subsurface waters ($\Delta\delta^{13}C_{DIC}$ = −0.49‰ to −0.57‰, average = -0.53 ± 0.04‰) and the core of SAMW ($\Delta\delta^{13}C_{DIC}$ = −0.13‰ to −0.57‰, average = −0.44 ± 0.05‰), with a more moderate shift in AAIW ($\Delta\delta^{13}C_{DIC}$ = +0.02‰ to −0.19‰, average = −0.11 ± 0.05‰). Density binned $\Delta\delta^{13}C_{DIC}$ data are shown in Table 2.

4.2. The ^{13}C Suess Effect and Anthropogenic Carbon Storage Within Subsurface Water Masses

The analyses of $\delta^{13}C_{DIC}$ and $\Delta\delta^{13}C_{DIC}$ in depth, T-S and density space outlined in Section 3.3. point to SAMW as the subsurface water mass most affected by the ^{13}C Suess effect in the SE Indian Ocean over the last 10 years. SAMW is produced when deep convection during austral winter leads to the formation of a mixed layer with vertically uniform density characteristics (i.e., a pycnostad), reaching up to 500 m deep (Dong et al., 2008; McCartney, 1977; Sallée et al., 2010). Northward advection of SAMW leads to subduction beneath subtropical waters with permanent thermoclines and isolation from seasonal air-sea gas exchange (Hasson et al., 2012; Rintoul et al., 2002). The southeastern Indian and Pacific Oceans are particularly strong regions of SAMW production (Cervoečki et al., 2013; McCartney, 1982; Hartin et al., 2011; Talley, 2013). Northward circulation of SAMW plays a critical role in ventilation and nutrient supply to the subtropical gyre thermocline waters within both the Indian and Pacific basins (Marinov et al., 2006; McCartney, 1982). A model tracer experiment of SAMW export suggests mode waters formed in the Indian Ocean are the fastest mode waters to exit the Southern Ocean, with ∼50% of SAMW exiting within 9 years (Jones et al., 2016). The same experiment found SAMW formed in the eastern Indian basin is also the quickest mode water to reach subtropical thermocline waters, with 83% of SAMW formed at −41°S in the experiment ventilating subtropical waters after just 50 years (Jones et al., 2016).

The southern Indian Ocean and Southern Ocean have demonstrated a long-term trend of subsurface warming since at least the 1950s (Hu & Fedorov, 2020; Yang et al., 2020). Within the Indian Ocean basin this warming signal is most prominent within the upper 400 m of the water column. This warming appears to be transmitted from the high latitude surface Southern Ocean to subsurface tropical latitudes with the

Indian basin along SAMW isopycnals, on timescales of ~10 years (Yang et al., 2020). The eMLR calculation used in this study takes into account changes in the temperature of water masses that may have occurred between 2008 and 2018, as it incorporates θ. However, a linear regression of the kind used in this analysis by its very nature will mute extreme signals. As a strongly temperature-dependent fractionation of carbon isotopes occurs during air-sea gas exchange, resulting in lower $\delta^{13}C_{DIC}$ values at higher temperatures (Zhang et al., 1995), it is conceivable that part of the $\Delta\delta^{13}C_{DIC}$ signal we observe may therefor result from the long-term warming of SAMW. An average decadal sea surface warming of 0.18°C per decade has been observed within the south-eastern Indian Ocean since 1950 (Hu & Fedorov, 2020). This warming is expected to yield a decrease in surface ocean $\delta^{13}C_{DIC}$ of −0.019‰ per decade (Zhang et al., 1995), an order of magnitude smaller than the change we observe. Furthermore, we see no evidence for warming within subsurface SAMW between 2008 and 2018 within our study region. It therefore appears unlikely that part of the $\Delta\delta^{13}C_{DIC}$ signal observed in this study is due to warming of SAMW between the study periods. We therefore rule out sea surface temperature changes within the formation region of SAMW as the primary driver of $\Delta\delta^{13}C_{DIC}$ within SAMW.

Immediately underlaying SAMW within our study region is AAIW. AAIW forms from cooler, more southerly surface waters than SAMW, in the region of the Polar Front (Sloyan & Rintoul, 2001). Absorption of atmospheric CO_2 into the surface ocean is partly temperature dependent, with higher CO_2 solubility at cooler temperatures. Furthermore, air-sea gas exchange within the region of the polar front is expected to be high due to the strong winds within the region, which promotes increased air-sea gas exchange. One might therefore expect a stronger expression of the ^{13}C Suess effect within AAIW that is sourced from colder and more turbulently mixed surface waters than in SAMW over the past decade, the opposite of what we observe. As AAIW in our study region was formed prior to SAMW, some of the difference in the magnitude of the oceanic ^{13}C Suess effect between these water masses is likely a function of lower atmospheric CO_2 concentrations and a smaller atmospheric ^{13}C Suess effect at the time of AAIW versus SAMW formation. However, this is likely to be a minor effect and cannot readily explain the 4-fold difference in oceanic ^{13}C Suess effect between the two water masses. A recent study of the global ^{13}C Suess effect and oceanic carbon inventory changes since the industrial revolution suggests that the difference in magnitude between the ^{13}C Suess effect in SAMW and AAIW can be attributed to differing degrees to which each water mass equilibrated with atmospheric CO_2 at the surface in their respective formation regions (Eide, Olsen, Ninnemann, & Johannessen, 2017). The study's authors suggest that a shorter surface ocean residence time of upwelled CDW south of the SAF and in the region of the PF causes less air-sea CO_2 exchange in the precursor surface waters of AAIW than is the case for SAMW. We similarly attribute the difference in the magnitude of ^{13}C Suess effect over the last decade between AAIW and SAMW to the much shorter residence time of AAIW versus SAMW precursor waters in the surface ocean, allowing a more complete equilibration of SAMW precursor surface waters with atmospheric CO_2. The $\Delta\delta^{13}C_{DIC}$ within the core of SAMW is 0.44 ± 0.05‰, slightly greater than—but just within error of—the atmospheric $\delta^{13}C$ change of ~0.39‰ across the same time period, suggesting the precursor surface waters of SAMW were in equilibrium with the atmosphere. It is worth noting that a more complete air-sea gas exchange within the surface waters which went onto form the SAMW within our study period (2018) than that of the CLIVAR period (2007–2009) could result in $\Delta\delta^{13}C_{DIC}$ values above and beyond the atmospheric change, making it hypothetically possible for SAMW $\Delta\delta^{13}C_{DIC}$ to exceed the atmospheric ^{13}C change.

Eide, Olsen, Ninnemann, and Eldevik (2017) calculated the slope between $\Delta\delta^{13}C_{DIC}$ and storage of anthropogenic carbon ($\Delta[C_{ant}]$) within the Indian Ocean since preindustrial times and found that it varied regionally and between isopycnal layers (i.e., between water masses). Using these slope estimates, we calculate $\Delta[C_{ant}]$ for given isopycnal ranges between 2007–2009 and 2018 within our study region (Table 2). These estimates of $\Delta[C_{ant}]$ suggest SAMW has played a dominant role in the sequestration of anthropogenic C within the ocean interior. Storage of anthropogenic carbon within the core of SAMW (σ_θ = 26.5–26.7) has increased by 55 ± 6 $\mu mol/kg^{-1}$ between 2007–2009 and 2018, which is an order of magnitude greater than the increase of 5 ± 2 $\mu mol/kg^{-1}$ within the core of AAIW (σ_θ = 27.1–27.3), estimated for the same time period. Eide, Olsen, Ninnemann, and Eldevik (2017) do not provide the uncertainty estimates associated with these slopes, so the uncertainty associated with these calculations is likely to be greater than quoted in this study.

4.3. Long-Term Trends in the ^{13}C Suess Effect and Storage of Anthropogenic Carbon in the SE Indian Ocean

We calculate an average surface water (0–49 m water depth) $\Delta\delta^{13}C_{DIC}$ value of −0.53 ± 0.04‰ in our study region across the last decade (Table 1). This surface ocean change is substantially higher than the average decadal change observed at the subtropical Pacific Hawaii Ocean Time Series of −0.25‰ per decade between 1991 and 2012 (Karl & Lukas, 1996), and the average decadal change of −0.24‰ at the Bermuda Time Series in the subtropical North Atlantic between 1983 and 2001 (Gruber et al., 2002; Quay et al., 2017). This calculated surface change is also higher than the surface ocean change of −0.28‰ per decade observed in Drake Passage between 55°S and 63°S from 2005 to 2014. (Munro et al., 2015; Quary et al., 2017). Quay et al. (2017) note that the decadal rate of $\delta^{13}C$ change in Drake Passage is significantly higher than expected if surface ocean air-sea pCO_2 and ^{13}C exchange occurred in equilibrium (−0.22‰ per decade), implying increased sequestration of anthropogenic ^{13}C and pCO_2. This is in line with other evidence for an increase in oceanic uptake of anthropogenic pCO_2 since the early 2000s (Gruber et al., 2019; Landschützer et al., 2015). Our calculated average surface ocean $\Delta\delta^{13}C_{DIC}$ of −0.53 ± 0.04‰ between 2008 and 2018 is also greater than the atmospheric $\delta^{13}C$ change of approximately −0.39‰ across the same time period. This offset between atmospheric and upper ocean $\Delta\delta^{13}C$ is unlikely to be due to a more complete air-sea gas exchange of surface waters in 2018 than was the case in 2008, as surface waters in this region are not quickly subducted, as is the case within AAIW and SAMW formation regions. This increased depletion in surface water $\Delta\delta^{13}C_{DIC}$ therefore suggests processes other than the oceanic ^{13}C Suess effect may have further lowered $\delta^{13}C_{DIC}$ of surface waters. An excess $\Delta\delta^{13}C_{DIC}$ above and beyond the atmospheric change could be due to an increase in the temperature of surface waters between 2008 and 2018, or a decline in export productivity within surface waters. The former seems unlikely, given that the average increase in sea surface temperatures within the southeastern Indian Ocean of 0.18°C per decade between 1950 and 2015 (Hu & Fedorov, 2020) can only account for a $\delta^{13}C_{DIC}$ change of −0.019‰ per decade (Zhang et al., 1995). The average $\Delta\delta^{13}C_{DIC}$ of −0.44 ± 0.05‰ within the core of SAMW over the last 10 years is less than the surface ocean within our study region. A $\Delta\delta^{13}C_{DIC}$ value of −0.44 ± 0.05‰ within SAMW is only slightly less than recently modeled changes for SAMW across the entire period from before the Industrial Revolution up to the mid-1990s, of c. −0.5 to −0.6‰ (Eide, Olsen, Ninnemann, & Eldevik, 2017; Eide, Olsen, Ninnemann, & Johannessen, 2017).

In order to investigate longer trends in the ^{13}C Suess effect within our study area, we utilize the same eMLR technique to model $\Delta\delta^{13}C_{DIC}$ between 1994/1995 and 2007–2009, using data collected as part of the World Ocean Circulation Experiment in 1994/1995 (triangles in Figure 1a; Talley et al., 2013) and applied to the CLIVAR data set ($\Delta\delta^{13}C_{DIC\text{-}CLIVAR}$). Calculated $\Delta\delta^{13}C_{DIC\text{-}CLIVAR}$ values in intermediate and deep waters (below c. 800 m) do not fall on the 0‰ line, but are instead shifted toward more ^{13}C-enriched values (Table 1 and Figure 5a). This shift cannot be explained by the oceanic ^{13}C Suess effect or by changes in the $\delta^{13}C$ of organic matter remineralization at depth resulting from the ^{13}C Suess effect, as these processes would both shift $\delta^{13}C_{DIC}$ the opposite direction (e.g., Lorrain et al., 2020). This shift may instead be due to a systematic bias or inter-laboratory offsets within the WOCE data set. The offset from zero averages 0.14‰ below 2,000 m water depth. We have therefore applied a uniform correction of 0.14‰ to all depth-binned $\Delta\delta^{13}C_{DIC\text{-}CLIVAR}$ values so that the data set could be compared with our $\Delta\delta^{13}C_{DIC}$ data. Annual $\Delta\delta^{13}C_{DIC}$ has then been calculated between 1994/95 (nominally 1994) and 2007–2009 (nominally 2008) and 2008–2018, to allow for direct comparison of rates of $\delta^{13}C_{DIC}$ change due to the ^{13}C Suess effect between the two time periods (Table 1, Figure 5b). Both WOCE-corrected and uncorrected data are presented, but values referred to in the text are calculated with a 0.14‰ correction applied, which consistently produces a larger annual change in $\Delta\delta^{13}C_{DIC}$ between 1994 and 2008.

The annual change in $\Delta\delta^{13}C_{DIC\text{-}CLIVAR}$ between 1994 and 2008 follows the same pattern with depth as the 2008–2018 data, with the greatest rate of change in surface waters (0–49 m, Table 1, Figure 5b). Both data sets show a decrease in annual $\Delta\delta^{13}C_{DIC}$ change down to ∼1,500 m water depth, below which the annual $\Delta\delta^{13}C_{DIC}$ change is within error of 0‰ per year at all depth bins. The greatest difference in annual rate of change in $\Delta\delta^{13}C_{DIC}$ between the two data sets is within the surface ocean, and reduces linearly with depth until c. 1,500 m water depth. Although the pattern is similar for both data sets, the rate of annual $\Delta\delta^{13}C_{DIC}$ change between 2008 and 2018 is greater at surface to intermediate depths than between 1994 and 2008, regardless of whether a correction of 0.14‰ is applied to the WOCE data set or not (Table 1, Figure 5b).

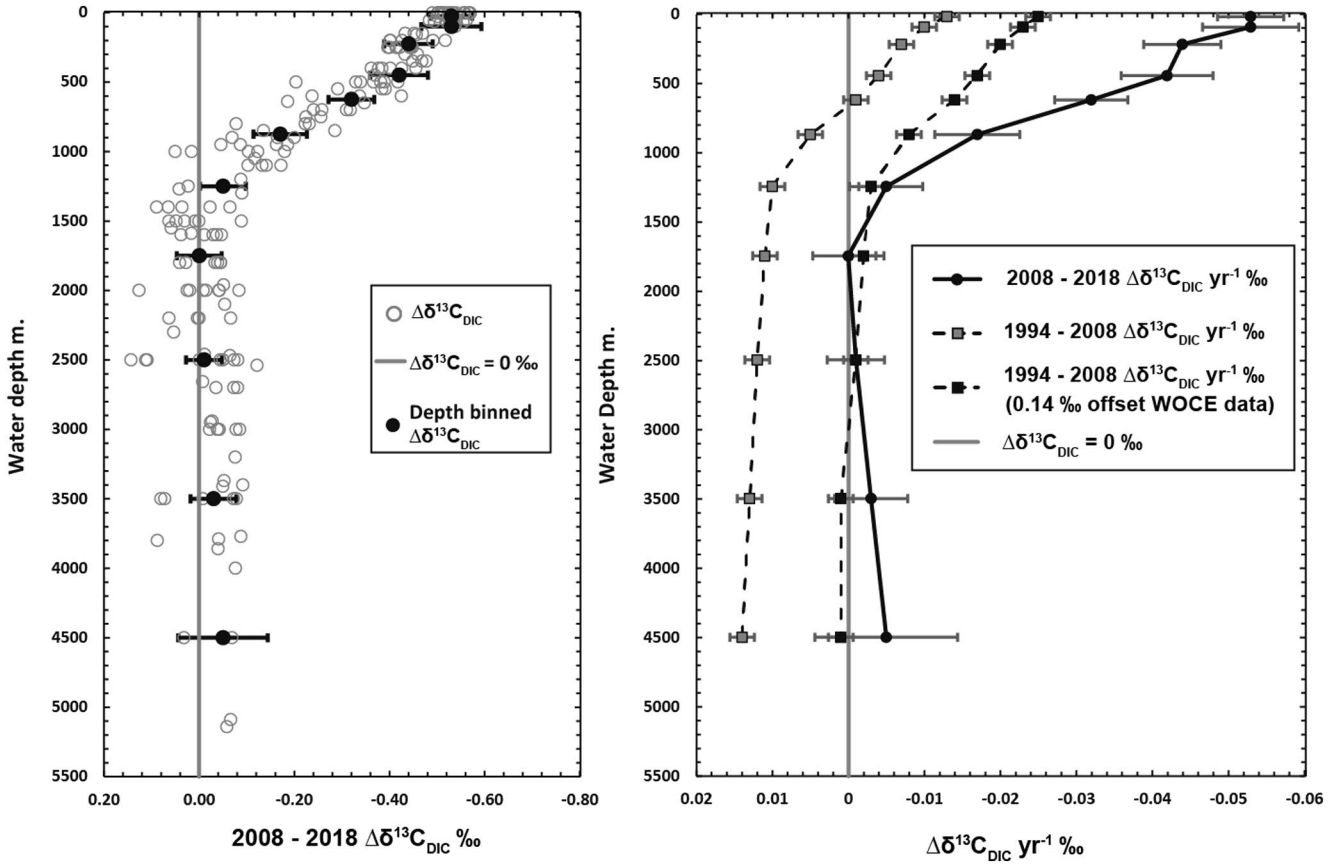

Figure 5. (a) Profile of oceanic ^{13}C Suess effect magnitude ($\Delta\delta^{13}C_{DIC}$) across all CROCCA-2S stations (gray dots) and depth-binned averages (black boxes). For depth ranges binned see Table 1. The largest $\Delta\delta^{13}C_{DIC}$ (-0.53 ± 0.04 to -0.53 ± 0.06‰) is observed between 0 and 149 m water depth. Data below c. 1,500 m fall within error of the $\Delta\delta^{13}C_{DIC} = 0$‰ line, that is, waters below this depth show no evidence for the oceanic ^{13}C Suess effect. This is expected for deeper water masses which have not been exposed to an atmosphere with elevated levels of anthropogenic CO_2 and suggests the eMLR technique does a good job at modeling $\delta^{13}C_{DIC}$ values. (b) Calculated annual change in $\Delta\delta^{13}C_{DIC}$ between 2008 and 2018 (circles and solid line), and 1994–2008 (squares and dashed line). The modeled change across 1994–2008 does not fall on the 0‰ line at depth. This offset averages 0.14‰ below 2,000 m. Even if a correction of 0.14‰ is applied to this data set (black squares line) to correct for this offset, the annual rate of change in the upper ocean between 1994 and 2008 is approximately half that observed between 2008 and 2018.

Using the relationship between $\delta^{13}C_{DIC}$ and $[C_{anth}]$ estimated by Eide, Olsen, Ninnemann, and Eldevik (2017), it is possible to estimate the annual storage of $[C_{anth}]$ between 1994 and 2008 within the water column (Table 3; see Section 3.4. above). Doing so yields an annual storage of $[C_{anth}]$ of $\sim 2.0 \pm 0.2$ μmol/kg per year within the core of SAMW (σ_θ = 26.5–26.7) across this time period. This is greater than a recent estimate of c. 1.0 μmol/kg/per year for the upper 500 m of the water column between −40°S and −30°S in the Indian Ocean between 1994 and 2007 (Gruber et al., 2019). Comparison with the density-binned change in $[C_{anth}]$ across 2008–2018 shows that the storage of anthropogenic carbon within the core of SAMW in the region of our study increased roughly 2–3 times, from 2.0 ± 0.2 μmol/kg per year between 1994 and 2008 to 5.5 ± 0.6 μmol/kg per year between 2008 and 2018 (Table 3).

SAMW ventilates the Indian Ocean subtropical thermocline on decadal timescales (Jones et al., 2016). The Indian Ocean subtropical thermocline today acts as a relatively small net source of CO_2 to the atmosphere (Bates et al., 2006). However, our estimate of a 2–3-fold increase in storage of $[C_{ant}]$ within SAMW over the last decade implies the rate of outgassing of anthropogenically sourced carbon from subtropical thermocline waters ventilated by SAMW is set to increase in the coming decades. The scale of this increase depends on the ability of SAMW to upwell and mix with thermocline waters within the subtropical Indian Ocean.

Previously published global estimates of anthropogenic carbon uptake rates spanning 1982–2011 suggest a slowdown during the 1990s, with uptake reaching a minimum in the late 1990s–early 2000s (Gruber

Table 3
Estimated Annual Uptake of Anthropogenic Carbon ($[C_{ant}]$) Between 1994–2008 and 2008–2018 for Different Density Layers, Using Relationship Between the Oceanic ^{13}C Suess Effect ($\Delta\delta^{13}C_{DIC}$) and $\Delta[C_{ant}]$ of Eide, Olsen, Ninnemann, and Eldevik (2017)

Potential density layer	2008–2018 $\Delta\delta^{13}C_{DIC}/yr^{-1}$	2008–2018 $\Delta[C_{ant}]$ μmol/kg^{-1}/yr^{-1}	1994–2008 $\Delta\delta^{13}C_{DIC}/yr^{-1}$	1994–2008 $\Delta[C_{ant}]$ μmol/kg^{-1}/yr^{-1}	Water mass
<26.5	−0.053 ± 0.004	–	−0.021 ± 0.002	–	Surface
26.5–26.7	−0.044 ± 0.005	5.5 ± 0.6	−0.016 ± 0.002	2.0 ± 0.2	SAMW
26.7–26.9	−0.033 ± 0.004	2.4 ± 0.3	−0.013 ± 0.002	0.9 ± 0.1	SAMW
26.9–27.1	−0.020 ± 0.008	0.8 ± 0.3	−0.007 ± 0.002	0.3 ± 0.1	SAMW/AAIW interface
27.1–27.3	−0.011 ± 0.005	0.5 ± 0.2	−0.003 ± 0.002	0.1 ± 0.1	AAIW
27.3–27.5	−0.001 ± 0.008	0.1 ± 0.5	0.000 ± 0.002	0.0 ± 0.1	CDW
27.5–27.7	0.000 ± 0.004	0.0 ± 0.2	0.001 ± 0.002	0.0 ± 0.1	CDW
>27.7	−0.002 ± 0.003	–	0.003 ± 0.002	–	CDW

Note. An offset of 0.14‰ is applied to $\Delta\delta^{13}C_{DIC}$ used in calculation of 1994–2008 as discussed in Section 3.5.

et al., 2019; Landschützer et al., 2015; Rodenbeck et al., 2014). Anthropogenic carbon uptake then increased to values in line with those expected from modeling studies in the early- to mid-2000s (H. D. Graven et al., 2012). This temporary decrease in oceanic CO_2 uptake has been linked to a southward shift in the southern hemisphere westerly wind belt and a hypothesized increase in Ekman transport and meridional overturning within the Southern Ocean (DeVries et al., 2017). The resulting strong overturning is suggested to have increased upwelling of DIC-rich CDW, reducing the capacity of surface waters to absorb CO_2. Conversely, the subsequent increase in oceanic carbon sequestration since the mid-2000s has been tied to a proposed slowdown in upper ocean overturning rates within the Southern Ocean (DeVries et al., 2017). However, recent analysis of Southern Hemisphere ARGO float data spanning 2005–2017 demonstrate that Ekman pumping within the region of SAMW formation has actually increased since the mid-2000s (Gao et al., 2018; Qu et al., 2020), leading to an increase in SAMW production. It therefore appears that the large increase in the magnitude of the oceanic Suess effect between 2008 and 2018 identified here cannot be accounted for by a slowdown in Ekman divergence, as suggested previously.

Published estimates, based on data collected up to 2011, for the strengthening of oceanic CO_2 uptake following the late 1990s to early 2000s minimum suggest a roughly 3-fold increase globally, from 0.8 ± 0.5 $PgCyr^{-1}$ to 2.0 ± 0.5 $PgCyr^{-1}$ (Landschützer et al., 2015, 2016). This represents an increase of the same order of magnitude as we observe in annual $[C_{anth}]$ storage rates between 1994–2008 and 2008–2018 (2–3-fold). Ours is the first data to confirm this estimate of increased uptake extends beyond 2011. Furthermore, we demonstrate that this increased uptake of anthropogenic CO_2 is greatest within SAMW and coincides with a period of increased SAMW production, rather than a slowdown in Southern Ocean overturning.

5. Conclusions

Fossil fuel usage has led to the accumulation of anthropogenic CO_2 in the atmosphere, with the rate of increase accelerating in recent decades (Raupach et al., 2007). The oceans are the largest sink of this anthropogenic CO_2, with the Southern Ocean responsible for ~40% of that uptake (Sabine et al., 2004). The shallow to intermediate waters forming within the high latitude SE Indian Ocean play a key role in sequestering this anthropogenic CO_2 (Eide, Olsen, Ninnemann, & Johannessen, 2017), and the subsurface SE Indian Ocean is therefore expected to be disproportionally affected by the oceanic ^{13}C Suess effect.

We assessed the magnitude of the oceanic ^{13}C Suess effect in the SE Indian Ocean across more than three decades by comparing past seawater $\delta^{13}C_{DIC}$ data collected in this region in previous surveys (spanning 1994–1995 and 2007–2009, nominally 1994 and 2008 respectively) with data collected during the CROCCA-2S cruise in 2018. The surface ocean and SAMW within the SE Indian Ocean have been disproportionately affected by the oceanic ^{13}C Suess effect. Between 2008 and 2018, $\delta^{13}C_{DIC}$ values shifted by an average of c. −0.53 ± 0.05‰ in the upper 150 m of the water column, −0.44 ± 0.05‰ within the main core of SAMW, and −0.11 ± 0.05‰ within AAIW. The rate of decrease within SAMW is one of the fastest changes attributed

to the oceanic ^{13}C Suess effect observed anywhere in the global ocean (e.g., Eide, Olsen, Ninnemann, & Johannessen, 2017; Quay et al., 2007). Comparison with earlier data demonstrates that our estimated rate of annual $\Delta\delta^{13}C$ within SAMW is 2–3 times higher than the period between 1994 to 2008. This large increase since 2008 partially reflects a previously identified slowdown in the uptake of anthropogenic CO_2 within the SE Indian and Southern Ocean during the late 1990s and early 2000s. Our calculations confirm that this slowdown was followed by an acceleration of CO_2 uptake from the mid-2000s onwards (Landschützer et al., 2015, 2016), and for the first time show that this increased uptake has been sustained through the 2010s as production of SAMW increased.

Using previous estimates of the relationship between $\Delta\delta^{13}C$ and uptake of anthropogenic carbon in the SE Indian Ocean (Eide, Olsen, Ninnemann, & Johannessen, 2017), we calculate that up to 55 ± 6 umol/kg^{-1} of additional anthropogenic carbon has been sequestered within SAMW between 2008 and 2018, that is, an excess storage of 5.5 ± 0.6 umol/kg^{-1} per year. The total increase in anthropogenic carbon storage within AAIW is estimated at 5 ± 2 umol/kg^{-1} (0.5 ± 0.2 umol/kg^{-1} per year) across the same time period. This represents a 2–3-fold increase in the rate at which anthropogenic carbon is sequestered within SAMW between 2008 and 2018, compared with the period from 1994 to 2008. As SAMW within our study region goes on to ventilate the subtropical thermocline on decadal timescales, the rate of outgassing of anthropogenic CO_2 from the subtropical thermocline within the Indian Ocean is therefore set to increase in the coming decades. The increased storage of anthropogenic carbon within SAMW over the last decade also coincides with an increase in the production and export of SAMW from the Southern Ocean. This concurrent increase in the production of SAMW and storage of anthropogenic carbon within it make SAMW a critical component of the ocean's ability to absorb anthropogenic carbon emissions. Ongoing work is therefore required to investigate the possible mechanisms for increased anthropogenic carbon storage over the last decade, including the continued long-term monitoring of seawater $\delta^{13}C_{DIC}$ within the Southern Ocean.

Data Availability Statement

Data produced as part of this work are available on the NOAA National Centers for Environmental Information website at https://doi.org/10.25921/7xxc-zk87.

Acknowledgments
We thank the officers, crew, and shipboard scientists aboard the R/V Thomas G. Thompson during the CORCCA-2S cruise of October–December 2018. We also thank J. Curtis and the Light Stable Isotope Mass Spec Lab team at the Department of Geological Sciences, University of Florida for performing the stable isotope analyses. This work forms part of the NSF award OCE-1559080 "Coring in the Southwest Indian and Southern Oceans to examine climate driven changes in watermass paleoventilation, sources, and structure," and was additionally supported by NSF award OCE-1737151 to C. Basak (Project tittle: "Testing the fidelity of neodymium isotopes as a paleocirculation tracer in the Southeast Indian-Southern Ocean"). This manuscript was greatly improved by comments and suggestions made by K. Gunn and an anonymous reviewer.

References

Bates, N. R., Pequignet, A. C., & Sabine, C. L. (2006). Ocean carbon cycling in the Indian Ocean: 1. Spatiotemporal variability of inorganic carbon and air-sea CO_2 gas exchange. *Global Biogeochemical Cycles*, *20*, GB3020. https://doi.org/10.1029/2005GB002491

Cervoečki, I., Talley, L. D., & Mazloff, M. R. (2013). Subantarctic mode water formation, destruction, and export in the eddy-permitting Southern Ocean state estimate. *Journal of Physical Oceanography*, *43*, 1485–1511. https://doi.org/10.1175/JPO-D-12-0121.1

DeVries, T., Holzer, M., & Primeau, F. (2017). Recent increase in oceanic carbon uptake driven by weaker upper-ocean overturning. *Nature*, *542*, 215–218. https://doi.org/10.1038/nature21068

Dlugokencky, E. J., Hall, B. D., Montzka, S. A., Dutton, G., Mühle, J., & Elkins, J. W. (2019). Atmospheric composition [*in State of the Climate in 2018*, Chapter 2: Global Climate]. *Bulletin of the American Meteorological Society*, *100*(9), S48–S50.

Dong, S., Sprintall, J., Gille, S. T., & Talley, L. (2008). Southern Ocean mixed-layer depth from Argo float profiles. *Journal of Geophysical Research*, *113*, C06013. https://doi.org/10.1029/2006JC004051

Eide, M., Olsen, A., Ninnemann, U. S., & Eldevik, T. (2017). A global estimate of the full oceanic ^{13}C Suess effect since the preindustrial. *Global Biogeochemical Cycles*, *31*, 492–514. https://doi.org/10.1002/2016GB005472

Eide, M., Olsen, A., Ninnemann, U. S., & Johannessen, T. (2017). A global ocean climatology of preindustrial and modern ocean $\delta^{13}C$. *Global Biogeochemical Cycles*, *31*, 515–534. https://doi.org/10.1002/2016GB005473

Feely, R. A., Dickson, A. G., Hansell, D. A., Wanninkhof, R., McNichol, A., & Key, R. M. (2013). Dissolved inorganic carbon (DIC), total alkalinity, pH on total scale, temperature, salinity and other variables collected from discrete sample and profile observations during the R/V Roger Revelle cruise CLIVAR_I05_2009 (EXPOCODE 33RR20090320) in the Indian Ocean from 2009-03-20 to 2009-05-15 (NCEI Accession 0108075). NOAA National Centers for Environmental Information. https://doi.org/10.3334/cdiac/otg.clivar_i05_2009

Feely, R. A., Sabine, C. L., Dickson, A. G., Wanninkhof, R., & Hansell, D. A. (2013). Dissolved inorganic carbon (DIC), total alkalinity, temperature, salinity and other variables collected from discrete sample and profile observations during the R/V Roger Revelle cruise CLIVAR_I08S_2007 (EXPOCODE 33RR20070204) in the Indian Ocean from 2007-02-04 to 2007-03-17 (NCEI Accession 0108119). NOAA National Centers for Environmental Information. https://doi.org/10.3334/cdiac/otg.clivar_i08s_2007

Feely, R. A., Sabine, C. L., Millero, F. J., Wanninkhof, R., & Hansell, D. A. (2013). Dissolved inorganic carbon (DIC), total alkalinity, pH on sea water scale, temperature, salinity and other variables collected from discrete sample and profile observations during the R/V Roger Revelle cruise CD139, CLIVAR I09N_2007 (EXPOCODE 33RR20070322) in the Indian Ocean from 2007-03-22 to 2007-05-01 (NCEI Accession 0110791. NOAA National Centers for Environmental Information. https://doi.org/10.3334/cdiac/otg.clivar_i09n_2007

Fine, R. A. (1993). Circulation of Antarctic intermediate water in the South Indian Ocean. *Deep Sea Research Part I: Oceanographic Research Papers*, *40*, 2021–2042. https://doi.org/10.1016/0967-0637(93)90043-3

Freeman, K. H., & Hayes, J. M. (1992). Fractionation of carbon isotopes by phytoplankton and estimates of ancient CO_2 levels. *Global Biogeochemical Cycles*, *6*, 185–198. https://doi.org/10.1029/92gb00190

Friis, K., Körtzinger, A., Pätsch, J., & Wallace, D. W. R. (2005). On the temporal increase of anthropogenic CO_2 in the subpolar North Atlantic. *Deep Sea Research Part I: Oceanographic Research Papers*, *52*, 681–698.

Gao, L., Rintoul, S. R., & Yu, W. (2018). Recent wind-driven change in Subantarctic Mode Water and its impact on ocean heat storage. *Nature Climate Change*, *8*(1), 51–63. https://doi.org/10.1038/s41558-017-0022-8

Graven, H., Allison, C. E., Etheridge, D. M., Hammer, S., Keeling, R. F., Levin, I., et al. (2017). Compiled records of carbon isotopes in atmospheric CO_2 for historical simulations in CMIP6. *Geoscientific Model Development*, *10*, 4405–4417. https://doi.org/10.5194/gmd-10-4405-2017

Graven, H. D., Gruber, N., Key, R., Khatiwala, S., & Giraud, X. (2012). Changing controls on oceanic radiocarbon: New insights on shallow-to-deep ocean exchange and anthropogenic CO_2 uptake. *Journal of Geophysical Research*, *117*, C10005. https://doi.org/10.1029/2012jc008074

Gruber, N., Clement, D., Carter, B. R., Feely, R. A., van Heuven, S., Hoppema, M., et al. (2019). The oceanic sink for anthropogenic CO_2 from 1994 to 2007. *Science*, *363*, 1193–1199. https://doi.org/10.1126/science.aau5153

Gruber, N., Keeling, C. D., Bacastow, R. B., Guenther, P. R., Lueker, T. J., Wahlen, M., et al. (1999). Spatiotemporal patterns of carbon-13 in the global surface oceans and the oceanic Suess effect. *Global Biogeochemical Cycles*, *13*, 307–335. https://doi.org/10.1029/1999gb900019

Gruber, N., Keeling, C. D., & Bates, N. R. (2002). Interannual variability in the North Atlantic Ocean carbon sink. *Science*, *298*(5602), 2374–2378. https://doi.org/10.1126/science.1077077

Hanawa, K., & Talley, L. D. (2001). Mode waters, in ocean circulation and climate. In G. Seidler, J. Church, & J. Gould (Eds.), *International Geophysical Series* (pp. 373–386). Academic Press.

Hartin, C. A., Fine, R. A., Sloyan, B. M., Talley, L. D., Chereskin, T. K., & Happell, J. (2011). Formation rates of Subantarctic mode water and Antarctic intermediate water within the South Pacific. *Deep Sea Research Part I: Oceanographic Research Papers*, *58*, 524–534. https://doi.org/10.1016/j.dsr.2011.02.010

Hasson, A., Koch-Larrouy, A., Morrow, R., Juza, M., & Penduff, T. (2012). The origin and fate of mode water in the southern Pacific Ocean. *Ocean Dynamics*, *62*(3), 335–354. https://doi.org/10.1007/s10236-011-0507-3

Hu, S., & Fedorov, A. V. (2020). Indian Ocean warming as a driver of the North Atlantic warming hole. *Nature Communications*, *11*, 4785. https://doi.org/10.1038/s41467-020-18522-5

Jones, D. C., Meijers, A. J. S., Shuckurgh, E., Sallée, J.-B., Haynesm, P., McAufield, E. K., & Mazloff, M. R. (2016). How does Subantarctic Mode Water ventilate the Southern Hemisphere subtropics? *Journal of Geophysical Research: Oceans*, *121*, 6558–6582. https://doi.org/10.1002/2016JC011680

Karl, D. M., & Lukas, R. (1996). The Hawaii Ocean Time-series (HOT) program: Background, rationale and field implementation. *Deep Sea Research Part II: Topical Studies in Oceanography*, *43*, 129–156. https://doi.org/10.1016/0967-0645(96)00005-7

Keeling, C. D., Mook, W. G., & Tans, P. P. (1979). Recent trends in the $^{13}C/^{12}C$ ratio of atmospheric carbon dioxide. *Nature*, *277*, 121–123. https://doi.org/10.1038/277121a0

Keeling, C. D., Piper, S. C., Bacastow, R. B., Wahlen, M., Whorf, T. P., Heimann, M., & Meijer, H. A. J. (2005). Atmospheric CO_2 and $^{13}CO_2$ exchange with the terrestrial biosphere and oceans from 1978 to 2000: Observations and carbon cycle implications. In J. R. Ehleringer, T. E. Cerling, & M. D. Dearing (Eds.), *A history of atmospheric CO_2 and its effects on plants, animals, and ecosystems*. (pp. 83–113). NewYork, NY: Springer Verlag.

Kroopnick, P. M. (1985). The distribution of ^{13}C of ΣCO_2 in the world oceans. *Deep-Sea Research Part A. Oceanographic Research Papers*, *32*, 57–84. https://doi.org/10.1016/0198-0149(85)90017-2

Landschützer, P., Gruber, N., & Bakker, D. C. E. (2016). Decadal variations and trends of the global ocean carbon sink. *Global Biogeochemical Cycles*, *30*, 1396–1417. https://doi.org/10.1002/2015GB005359

Landschützer, P., Gruber, N., Haumann, F. A., Rödenbeck, C., Bakker, D. C. E., van Heuven, S., et al. (2015). The reinvigoration of the Southern Ocean carbon sink. *Science*, *349*, 1221–1224. https://doi.org/10.1126/science.aab2620

Locarnini, R. A., Mishonov, A. V., Antonov, J. I., Boyer, T. P., Garcia, H. E., Baranova, O. K., et al. (2013). World Ocean Atlas 2013, Volume 1. *Temperature*. S. Levitus, Ed., A. Mishonov, Technical Ed. NOAA Atlas NESDIS 73, 40 pp.

Lorrain, A., Pethybridge, H., Cassar, N., Receveur, A., Allain, V., Bodin, N., et al. (2020). Trends in tuna carbon isotopes suggest global changes in pelagic phytoplankton communities. *Global Change Biology*, *26*, 458–470. https://doi.org/10.1111/gcb.14858

Marinov, I., Gnanadesikan, A., Toggweiler, J. R., & Sarmiento, J. L. (2006). The Southern Ocean biogeochemical divide. *Nature*, *441*, 964–967. https://doi.org/10.1038/nature04883

McCartney, M. S. (1977). Subantarctic mode water. In M. V. Angel (Ed.), *A voyage of discovery deep-sea research (suppl.)* (pp. 103–119). Oxford, UK: Pergammon.

McCartney, M. S. (1982). The subtropical recirculation of mode waters. *Journal of Marine Research*, *40*, 427–464.

McCartney, M. S., & Donohue, K. A. (2007). A deep cyclonic gyre in the Australian-Antarctic Basin. *Progress in Oceanography*, *75*(4), 675–750. https://doi.org/10.1016/j.pocean.2007.02.008

McNeil, B. I., Matear, R. J., & Tilbrook, B. (2001). Does carbon 13 track anthropogenic CO_2 in the southern ocean? *Global Biogeochemical Cycles*, *15*(3), 597–613. https://doi.org/10.1029/2000GB001352

Metzl, N., & Lo Monaco, C. (2018). Sea surface measurements of dissolved inorganic carbon (DIC), total alkalinity (TALK), temperature and salinity during the R/V Marion-Dufresne Ocean Indien Service d'Observations - 17 (OISO-17) cruise (EXPOCODE 35MV20090104) in the Indian Ocean from 2009-01-04 to 2009-02-09 (NCEI Accession 0173572). NOAA National Centers for Environmental Information. https://doi.org/10.7289/v5rr1wjt

Munro, D. R., Lovenduski, N. S., Stephens, B. B., Newberger, T., Arrigo, K. R., Takahashi, T., et al. (2015). Estimates of net community production in the Southern Ocean determined from time series observations (2002-2011) of nutrients, dissolved inorganic carbon, and surface ocean pCO_2 in Drake Passage. *Deep Sea Research Part II: Topical Studies in Oceanography*, *114*, 49–63. https://doi.org/10.1016/j.dsr2.2014.12.014

O'Leary, M. H. (1981). Carbon isotope fractionation in plants. *Phytochemistry*, *20*(4), 553–567. https://doi.org/10.1016/0031-9422(81)85134-5

Qu, T., Gao, S., & Fine, R. A. (2020). Variability of the Sub-Antarctic Mode water subduction rate during the Argo Period. *Geophysical Research Letters*, *47*, e2020GL088248. https://doi.org/10.1029/2020GL088248

Quay, P., Sonnerup, R., Munro, D., & Sweeney, C. (2017). Anthropogenic CO_2 accumulation and uptake rates in the Pacific Ocean based on changes in the $^{13}C/^{12}C$ of dissolved inorganic carbon. *Global Biogeochemical Cycles*, *31*, 59–80. https://doi.org/10.1002/2016GB005460

Quay, P., Sonnerup, R., Stutsman, J., Maurer, J., Körtzinger, A., Padin, X. A., & Robinson, C. (2007). Anthropogenic CO_2 accumulation rates in the North Atlantic Ocean from changes in the $^{13}C/^{12}C$ of dissolved inorganic carbon. *Global Biogeochemical Cycles*, *21*, GB1009. https://doi.org/10.1029/2006GB002761

Quay, P., Sonnerup, R., Westby, T., Stutsman, J., & McNichol, A. (2003). Changes in the $^{13}C/^{12}C$ of dissolved inorganic carbon in the ocean as a tracer of anthropogenic CO_2 uptake. *Global Biogeochemical Cycles*, *17*, 4-1–4-20. https://doi.org/10.1029/2001GB001817

Quay, P. D., Tilbrook, B., & Wong, C. S. (1992). Oceanic uptake of fossil fuel CO_2: Carbon-13 evidence. *Science*, *256*, 74–79. https://doi.org/10.1126/science.256.5053.74

Raupach, M. R., Marland, G., Ciais, P., Le Quéré, C., Canadell, J. G., Klepper, G., & Field, C. B. (2007). Global and regional drivers of accelerating CO_2 emissions. *Proceedings of the National Academy of Sciences of the United States of America*, *104*, 10288–10293. https://doi.org/10.1073/pnas.0700609104

Rintoul, S. R., & England, M. H. (2002). Ekman transport dominates local air-sea fluxes in driving variability of SUBANTARCTIC MODE WATER. *Journal of Physical Oceanography*, *32*(5), 1308–1321. https://doi.org/10.1175/1520-0485(2002)032<1308:etdlas>2.0.co;2

Rödenbeck, C., Bakker, D. C. E., Metzl, N., Olsen, A., Sabine, C., Cassar, N., et al. (2014). Interannual sea-air CO_2 flux variability from an observation-driven ocean mixed-layer scheme. *Biogeosciences*, *11*, 4599–4613. https://doi.org/10.5194/bg-11-4599-2014

Sabine, C. L., Feely, R. A., Gruber, N., Key, R. M., Lee, K., Bullister, J. L., et al. (2004). The oceanic sink for anthropogenic CO_2. *Science*, *305*, 367–371. https://doi.org/10.1126/science.1097403

Sallée, J. B., Speer, K. G., & Rintoul, S. R. (2010). Zonally asymmetric response of the Southern Ocean mixed-layer depth to the Southern Annular Mode. *Nature Geoscience*, *3*, 273–279. https://doi.org/10.1038/ngeo812

Schlitzer, R. (2019). *Ocean data view*. Retrieved from http://odv.awi.de

Sloyan, B. M., & Rintoul, S. R. (2001). The Southern ocean limb of the global deep overturning circulation. *Journal of Physical Oceanography*, *31*, 143–173. https://doi.org/10.1175/1520-0485(2001)031<0143:tsolot>2.0.co;2

Sonnerup, R. E., Quay, P. D., & McNichol, A. P. (2000). The Indian Ocean ^{13}C Suess effect. *Global Biogeochemical Cycles*, *14*(3), 903–916. https://doi.org/10.1029/1999GB001244

Sonnerup, R. E., Quay, P. D., McNichol, A. P., Bullister, J. L., Westby, T. A., & Anderson, H. L. (1999). Reconstructing the oceanic ^{13}C Suess effect. *Global Biogeochemical Cycles*, *13*(4), 857–872. https://doi.org/10.1029/1999GB900027

Talley, L. (2013). Closure of the global overturning circulation through the Indian, Pacific, and Southern Oceans: Schematics and transports. *Oceanography*, *26*(1), 80–97. https://doi.org/10.5670/oceanog.2013.07

Talley, L. D., Pickard, G. L., Emery, W. J., & Swift, J. H. (2011). *Descriptive physical oceanography: An introduction* (6th ed.). Boston, MA: Elsevier.

Talley, L. D., Sparrow, M., Chapman, P., & Gould, J. (2013). Hydrographic Atlas of the World Ocean Circulation Experiment (WOCE). In M. Sparrow, P. Chapman, & J. Gould (Eds.), *Volume 4: Indian Ocean*. Southampton, UK: International WOCE Project Office.

Tamsitt, V., Talley, L. D., & Mazloff, M. R. (2019). A deep eastern boundary current carrying Indian Deep Water south of Australia. *Journal of Geophysical Research: Oceans*, *123*(3), 2218–2238. https://doi.org/10.1029/2018JC014569

Tans, P. P., Berry, J. A., & Keeling, R. F. (1993). Oceanic $^{13}C/^{12}C$ observations: A new window on ocean CO_2 uptake. *Global Biogeochemical Cycles*, *7*, 353–368. https://doi.org/10.1029/93GB00053

Wallace, D. W. R. (1995). *Monitoring global ocean carbon inventories* (OOSDP Background Report No. 5). Texas A&M University, College Station, TX.

Yang, L., Murtugudde, R., Zhou, L., & Liang, P. (2020). A potential link between the Southern Ocean warming and the South Indian Ocean heat balance. *Journal of Geophysical Research: Oceans*, *125*, e2020JC016132. https://doi.org/10.1029/2020JC016132

Zhang, J., Quay, P. D., & Wilbur, D. O. (1995). Carbon isotope fractionation during gas-water exchange and dissolution of CO_2. *Geochimica et Cosmochimica Acta*, *59*, 107–114. https://doi.org/10.1016/0016-7037(95)91550-d